Simulations of droplet coalescence in simple shear flow

Orest Shardt,*,† J.J. Derksen,† and Sushanta K. Mitra‡

Department of Chemical and Materials Engineering, University of Alberta, Edmonton, Canada, and Department of Mechanical Engineering, University of Alberta, Edmonton, Canada

E-mail: shardt@ualberta.ca

Abstract

Simulating droplet coalescence is challenging because small-scale (tens of nanometers) phenomena determine the behaviour of much larger (micron- to millimetre-scale) droplets. In general, liquid droplets colliding in a liquid medium coalesce when the capillary number is less than a critical value. We present simulations of droplet collisions and coalescence in simple shear flow using the free-energy binary-liquid lattice Boltzmann method. In previous simulations of low-speed collisions, droplets coalesced at unrealistically high capillary numbers. Simulations of non-coalescing droplets have not been reported, and therefore the critical capillary number for simulated collisions was unknown. By simulating droplets with radii up to 100 lattice nodes, we determine the critical capillary number for coalescence and quantify the effects of several numerical and geometric parameters. The simulations were performed with a well-resolved interface, a Reynolds number of one, and capillary numbers from 0.01 to 0.2. The ratio of the droplet radius and interface thickness has the greatest effect on the critical capillary number. As in experiments, the critical capillary number decreases with increasing droplet size. A second numerical parameter, the interface diffusivity (Péclet number)

*To whom correspondence should be addressed
†University of Alberta, Chemical Engineering
‡University of Alberta, Mechanical Engineering

also influences the conditions for coalescence: coalescence occurs at higher capillary numbers with lower Péclet numbers (higher diffusivity). The effects of the vertical offset between the droplets and the confinement of the droplets were also studied. Physically reasonable results were obtained and provide insight into the conditions for coalescence. Simulations that match the conditions of experiments reported in the literature remain computationally impractical. However, the scale of the simulations is now sufficiently large that a comparison with experiments involving smaller droplets ($\approx 10\mu$m) and lower viscosities ($\approx 10^{-6}$m^2/s, the viscosity of water) may be possible. Experiments at these conditions are therefore needed to determine the interface thickness and Péclet number that should be used for predictive simulations of coalescence phenomena.

Introduction

Predicting and understanding the conditions for droplet coalescence are important for many applications. At a large scale, emulsions, which consist of drops of one fluid dispersed in another, may be subjected to complex turbulent flows for example during mixing. In such a flow, droplets are sheared and collide, causing breakup and coalescence. The result of these interactions is a particular droplet size distribution.[1–3] Since macroscopic properties, such as the effective viscosity of an emulsion, and mass transfer rates between the fluids depend on the droplet size distribution, it is useful to predict how flow conditions change droplet sizes. To make such predictions, an understanding of when drops break up and coalesce is required. In addition to emulsion flows in large vessels and process equipment, droplet interactions are also important in microfluidic devices in which individual droplets can be formed and manipulated.[4–6] For example, droplets can be formed by injecting one liquid into another in a T-junction or the nozzle of a flow-focusing device.[4,5] Microfluidic devices can be used to study coalescence directly, and Bremond et al.[7] found that droplets coalesce when separating rather than when they are compressed.

Droplet collisions in shear flow have been studied by several authors. Guido and Simeone[8] used optical microscopy to measure droplet trajectories during collisions in simple shear. They did

not, however, determine the conditions for coalescence. Leal and co-workers[9–12] used a four-roll mill to determine the conditions for coalescence under varying system parameters. Their results are for predominantly extensional flows (flows with streamlines towards and away from a stagnation point), rather than simple shear flows. More recently, Chen et al.[13] studied the effect of confinement on droplet coalescence in simple shear. The experimental results identify parameter ranges over which the transition from coalescence to non-coalescence occurs, and they are useful for comparisons with simulations. In general, there are two motivations for using simulations to study coalescence. The first reason is to gain an understanding of coalescence by obtaining data and using initial conditions that are experimentally impractical. The second reason is to verify the accuracy of the simulation method so that simulations of coalescence in more complex systems can be used to predict or optimize the performance of that system. For example, simulations of polydisperse emulsion flows must correctly model the dependence of the conditions for coalescence on the size of the droplets.

The outcome of a droplet collision is a macroscopic event that depends on phenomena at a much shorter length-scale.[14] As two droplets approach, the fluid between them drains. If this drainage continues long enough and the film between the droplets becomes sufficiently thin, attractive intermolecular forces across the film dominate and a bridge forms between the droplets. This bridge grows due to capillary forces, and the droplets coalesce. For a surfactant-free mixture of two polymers, such as the polydimethylsiloxane (PDMS) and polyisobutylene (PIB) studied by Chen et al.,[13] van der Waals forces determine the minimum film thickness before a bridge forms. An order-of-magnitude estimate of this critical thickness is 27 nm.[13] In comparison, typical droplet diameters in emulsions and microfluidic devices range from 1 to 500μm, factors of 37 to 18500 times larger than this sample critical film thickness.

The range of length scales poses significant challenges for fully resolved simulations of droplet collisions and coalescence. When simulating such a system, one must use an exceedingly fine uniform mesh, a non-uniform mesh with significant refinement in the vicinity of interacting interfaces, or multi-scale modelling that incorporates the effects of phenomena at a small scale

into larger more coarsely-resolved simulations. In general, simulations of droplets have been performed using interface-tracking or interface-capturing methods.[15] Interface-tracking methods use meshes or other computational elements that lie on the interface. In these methods, the interface is "sharp" because fluid properties vary discontinuously over the interface. Examples of interface-tracking methods include the boundary integral, finite element, and immersed-boundary methods.[15] Loewenberg and Hinch[16] used the boundary integral method to simulate binary drop collisions in shear flow. They did not, however, include attractive forces in the simulations and did not therefore simulate coalescence. The boundary integral method has also been used to study the flow of concentrated emulsions[17,18] in periodic domains and model porous media.[19] Simulating topological changes, i.e. breakup and coalescence, in interface-tracking methods is computationally challenging due to the mesh transformation that must be performed. The methods also require a somewhat arbitrary choice about the distance when two interfaces are close enough that they should merge or pinch-off. Such a critical distance may not actually be a constant; Leal[11] notes the critical film thickness may depend on the droplet radius. Because a length-scale must be provided as an input to the model, the use of these simulation methods requires prior knowledge of this length, making the methods non-predictive.

Unlike interface-tracking methods, interface-capturing methods do not explicitly describe the position of the interface. Instead, a scalar identifies regions of different composition and the interface is located where this scalar equals a constant value that is typically zero or one half. Fluid properties vary continuously over the diffuse interface between two fluids. Examples of such methods include lattice Boltzmann, level-set, volume-of-fluid (VoF), and phase field models.[15] Changes in interface topology are handled automatically by these methods. However, it is necessary to understand the conditions when these changes (breakup and coalescence) occur in simulations and if the conditions match experiments. In some interface-capturing methods, the critical distance between interfaces for coalescence and breakup is determined by the grid, in contrast to the arbitrary (but specified) critical distance for interface-tracking methods. In the VoF and level-set methods, two interfaces connect when the chosen grid cannot resolve the gap between them (see e.g. Tryg-

gvason et al.[20]). For example, the VoF method aims at simulating non-interacting sharp interfaces. As Zaleski et al.[21] mention, a cutoff length-scale is introduced and interfacial physics below this length scale are ignored. The cells in the simulation domain have compositions of zero or one, except those cells that contain an interface. In these cells, the composition varies continuously between zero and one. The interfaces of colliding droplets connect when the chosen grid resolution can no longer resolve the two interfaces. Consequently, the conditions for coalescence are expected to depend on the cell size, though a detailed analysis, analogous to the present lattice Boltzmann method (LBM) work, is required to confirm the nature of the dependence. Grid-dependence is expected because the film between two droplets is resolved better as the mesh is refined, decreasing the critical thickness for rupture. As a result, a longer time is needed for the film to drain before rupturing. Coalescence would therefore occur later in higher-resolution simulations. In contrast, as we show in the "Interface resolution" section, we obtain grid-independent results with high-resolution free-energy LBM simulations. Similar results are expected with other phase-field methods, but LBMs are convenient to parallelize, making high-resolution simulations practical.

Lattice Boltzmann methods have seen much popularity for simulating microfluidic flows.[22] While several multiphase and multicomponent LBMs have been proposed, we focus on the binary-liquid free-energy method[23] due to its thermodynamic treatment of fluid mixtures. Simulations of droplet formation have been successful[24] with this method, and the deformation and breakup of droplets has been studied in detail to determine the numerical parameters that are required for accurate simulations.[25] The conditions for coalescence, however, have not been studied in detail, though other researchers have noted that droplets coalesce too easily.[26] While droplet coalescence in microfluidic devices has been studied experimentally,[6,7,27,28] it is not currently possible to predict such coalescence phenomena with simulations. The need to study simulations of droplet coalescence in detail is underscored by the development of non-coalescing emulsion models by several researchers.[29,30] Though these models can be used for flow conditions when coalescence does not occur, such models with suppressed coalescence cannot be used to study the transition to coalescence. Therefore, there is a need to characterize the coalescence behaviour of existing simu-

lation models, investigate the previously-noted discrepancy between simulations and experiments, and determine whether conditions can be found in which droplets do not coalesce.

Due to the thermodynamic treatment of the diffuse interface, i.e. the use of a Cahn-Hilliard fluid model, the behaviour of fluid interfaces in the free-energy LBM can be related to van der Waals forces. This is an important advantage over other methods in which a specified length or the grid resolution determines the conditions for coalescence. The connection between the free-energy model and interfacial forces has been explained, for example, by Yue et al.[31], who studied coalescence after a head-on collision with a spectral phase-field method. Dupuy et al.[32] used an LBM with a Cahn-Hilliard free-energy model to study the coalescence of liquid droplet pairs in vapour. Premnath and Abraham[33,34] also studied liquid droplets in vapour, but considered both head-on and off-centre collisions. They showed several cases of coalescence and splitting after temporary coalescence, but no cases where the interfaces never merged. The results agreed with experimental findings. Their work, however, is in the high Reynolds number regime ($\mathrm{Re} \approx 50$), and the easy coalescence noted by Jia et al.[26] occurs at low Reynolds numbers ($\mathrm{Re} < 1$). Different LBMs, i.e. other than the free-energy LBM, have also been used to study droplet collisions at high Reynolds numbers. Inamuro et al.[35], Lee and Lin[36], and Sun et al.[37] focused on achieving high density ratios between the liquid and vapour phases. Chiappini et al.[38] used a (two-dimensional) finite-difference lattice Boltzmann method[36] to study the Rayleigh-Taylor instability, droplet breakup, and droplet coalescence, while Lycett-Brown et al.[39] studied collisions with an improved Shan-Chen[40] LBM for liquid-vapour systems. To the authors' knowledge, studies of droplet collisions in liquid-liquid systems that are similar to those for liquid-vapour systems have not been reported. Perlekar et al.[41] studied large numbers of droplets (approximately 10 to 50) in turbulence using the Shan-Chen method, but the behaviour of a colliding pair of droplets was not investigated. Interestingly, simulations of droplet collisions and coalescence using the colour-model LBM,[42,43] the third LBM model that is commonly used for multiphase simulations, have not been reported. Simulations of deformation and breakup[44] and droplet formation in a microfluidic channel[45,46] have been described. Due to this success, the colour-model LBM may be a good candidate for coales-

cence simulations, but a comparison of coalescence behaviour in the colour-model and free-energy LBMs is beyond the scope of the current work. It should be noted that a link between numerical interface parameters in the color-model LBM and intermolecular forces is not immediately evident, suggesting a disadvantage of this model in comparison to the free-energy method.

In this work, we quantify the conditions for coalescence in the free-energy LBM during collisions of two liquid droplets in a liquid matrix. The Reynolds number is fixed at one, a low value that is efficient to simulate with this explicit numerical method. We determine the effects of droplet size, diffuse interface thickness, interface diffusivity, vertical offset between the droplets, and droplet confinement. This information is important for knowing the conditions when simulations of multiphase microfluidic flows and fully-resolved simulations of emulsions in turbulence correctly model droplet coalescence.

Coalescence Theory

A schematic of the coalescence problem that we simulate is shown in Fig. 1. Two initially spherical droplets of radius R are initialized with a horizontal distance ΔX and a vertical distance ΔY between their centres in a domain with a height H between the shear planes. A shear flow with a rate $\dot{\gamma} = \frac{2u_0}{H}$, where u_0 is the horizontal speed of the two shear planes, is started impulsively. The interfacial tension (or energy) between the droplet liquid and the surrounding liquid is σ. We do not currently study the effects of density or viscosity differences between the two liquids. Both liquids therefore have the same density ρ and kinematic viscosity ν. A domain with a finite length L and a finite depth W is used to represent a domain that is infinite in these dimensions. Thus the domain size is chosen to be large enough that the effects of the finite size can be neglected, and the adequacy of the choice is verified in the section "Domain size effect." To use available computational resources efficiently, we use symmetry boundary conditions and simulate only one quarter of the whole system as shown in Fig. 1.

The physical parameters give rise to several non-dimensional parameters. Hydrodynamic sim-

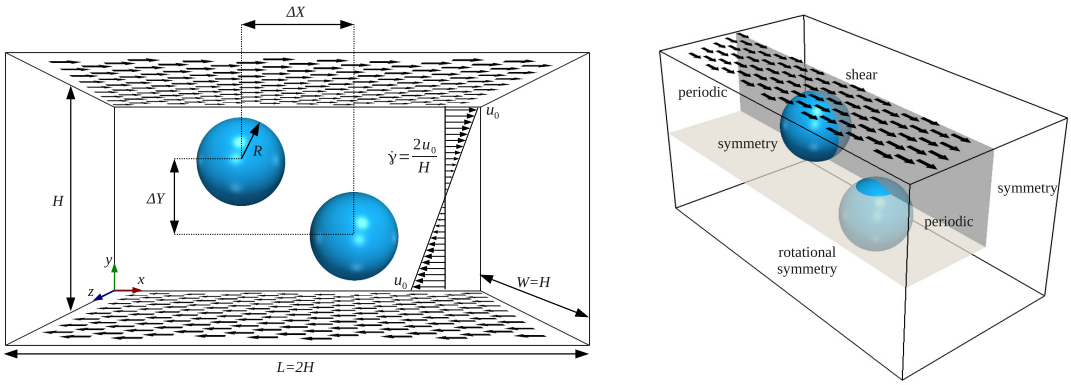

Figure 1: Schematics of the system geometry (left) and simulation domain (right). Two droplets with radii R are located between two shear planes that are a distance H apart and move at a speed u_0 in opposite directions. The horizontal (parallel to the shear planes) distance between the centres of the droplets is ΔX; the vertical distance is ΔY. The definitions of the coordinate axes and domain dimensions are also provided. Due to the symmetry of the full system (left), only one quarter is simulated (right). The boundary conditions on each face of the simulated domain are shown.

ilarity is specified by the Reynolds number Re, which we define using the characteristic velocity $\dot{\gamma}R$ and the droplet radius R as the characteristic length:

$$\mathrm{Re} \equiv \frac{\dot{\gamma}R^2}{\nu} \tag{1}$$

The effects of surface tension are captured by the capillary number Ca, which is the ratio of viscous ($\mu\dot{\gamma}R^2$) and interfacial (σR) forces:

$$\mathrm{Ca} \equiv \frac{\mu\dot{\gamma}R}{\sigma} \tag{2}$$

where $\mu = \rho\nu$ is the dynamic viscosity of both fluids. The geometric parameters are the confinement $\frac{2R}{H}$, the horizontal separation $\frac{\Delta X}{2R}$, and the vertical offset $\frac{\Delta Y}{2R}$.

The outcome of a collision is determined by the capillary number. With increasing capillary number, the deformation of droplets increases as the interfacial forces that keep a drop spherical give way to the viscous forces that shear the droplet. When droplets are deformable, their interfaces flatten when they are pushed together in a shear flow. The fluid film that forms between the droplets must drain before the interfaces can come close enough that intermolecular forces dominate and the interfaces merge. If the film does not thin sufficiently over the time of a collision, the drops

slide over each other; otherwise they coalesce. As the capillary number decreases, the reduced deformability of the droplets suppresses the formation of a flat film. In the limit of high surface tension ($\mathrm{Ca} \ll 1$), the drops would remain effectively spherical and a flat film could not form to delay coalescence. Thus, droplets cannot coalesce when the capillary number is sufficiently high and they coalesce when it is sufficiently low. There is therefore a critical capillary number Ca_c, and droplets coalesce when $\mathrm{Ca} < \mathrm{Ca}_c$; they slide when $\mathrm{Ca} > \mathrm{Ca}_c$.

The outcome of a collision is determined by hydrodynamic, capillary, and geometric effects, as well as a characteristic length scale l_c at which intermolecular forces become important and destabilize the thin film that separates colliding droplets. The dependence of these factors on the critical capillary number can be expressed as

$$\mathrm{Ca}_c = \mathrm{Ca}_c \left(\mathrm{Re}, \frac{\Delta X}{2R}, \frac{\Delta Y}{2R}, \frac{2R}{H}, \frac{R}{l_c} \right) \tag{3}$$

Numerical Method

We use the free-energy lattice Boltzmann method for binary liquid mixtures.[23] In this method, two discrete density distributions f_i and g_i model the hydrodynamics and the evolution of a phase field, respectively. A brief overview of the method is provided here to establish the definitions that are required for this paper; more details about the method and theory can be found elsewhere.[22–24,47–50] In general, lattice Boltzmann methods solve advection-diffusion equations through a two-step process that mimics the behaviour of molecules in a gas. In the first step, the densities at each lattice node are propagated to adjacent nodes along a set of discrete directions $\vec{c}_i$, where i identifies the discrete direction. We use a three-dimensional lattice with 19 discrete directions, i.e. a D3Q19 lattice, for both density fields. The second step imitates the effect of collisions between molecules by relaxing the densities at each node towards an equilibrium distribution. Thus, the density dis-

tributions f_i and g_i evolve according to

$$f_i(\vec{x}+\vec{c}_i\Delta t, t+\Delta t) = \left(1-\frac{1}{\tau_f}\right) f_i(\vec{x},t) + \frac{1}{\tau_f} f_i^{eq}(\vec{x},t) \tag{4}$$

$$g_i(\vec{x}+\vec{c}_i\Delta t, t+\Delta t) = \left(1-\frac{1}{\tau_g}\right) g_i(\vec{x},t) + \frac{1}{\tau_g} g_i^{eq}(\vec{x},t) \tag{5}$$

where τ_f and τ_g specify the relaxation rates. By relating macroscopic values to the density distributions and appropriately choosing the equilibrium distributions f_i^{eq} and g_i^{eq}, the simulations model the required continuum equations. For the f_i field, the macroscopic density and momentum are

$$\rho = \sum_i f_i \tag{6}$$

$$\rho\vec{u} = \sum_i f_i\vec{c}_i \tag{7}$$

and the equilibrium distribution is

$$f_i^{eq} = A_i + B_i\vec{u}\cdot\vec{c}_i + C_i\vec{u}\cdot\vec{u} + D_i(\vec{u}\cdot\vec{c}_i)^2 + G_{i,\alpha\beta}c_{i,\alpha}c_{i,\beta} \tag{8}$$

where index notation has been used for the last term and summation over repeated Greek indices is implied. The coefficients A_i, B_i, C_i, D_i and G_i must satisfy conservation constraints, but these constraints do not determine the coefficients uniquely. We use coefficients that minimize spurious currents.[51] With these definitions of the macroscopic variables and equilibrium function, the f_i field simulates the mass conservation (continuity) equation

$$\frac{\partial\rho}{\partial t} + \nabla\cdot(\rho\vec{u}) = 0 \tag{9}$$

and the incompressible Navier-Stokes equation

$$\frac{\partial\vec{u}}{\partial t} + (\vec{u}\cdot\nabla)\vec{u} = -\frac{1}{\rho}\nabla P + \nu\nabla^2\vec{u} \tag{10}$$

where the pressure is determined with the equation of state $P = \frac{1}{3}\rho$ and the kinematic viscosity is related to the relaxation rate by $\nu = \frac{1}{3}\left(\tau_f - \frac{1}{2}\right)$. To simulate incompressible flow, flow speeds must be kept low, and we achieve this by limiting the shear speed to approximately 0.02 lattice units per timestep.

For the phase field, the scalar ϕ specifies the composition of the fluid, and it varies between -1 (continuous phase) and 1 (droplet phase). It is determined from the density distribution g_i by

$$\phi = \sum_i g_i \tag{11}$$

The continuum equation for ϕ is

$$\frac{\partial \phi}{\partial t} + \nabla \cdot (\phi \vec{u}) = M \nabla^2 \mu \tag{12}$$

In this advection-diffusion equation for ϕ, M is the diffusivity of the chemical potential μ. This diffusivity is determined by the relaxation time τ_g and a free parameter Γ according to $M = \Gamma\left(\tau_g - \frac{1}{2}\right)$, while the chemical potential is determined by the free-energy of the system. The free-energy functional $F[\phi(\vec{x})]$ is[23]

$$F = \int_V \left[\frac{1}{3}\rho \ln \rho + \frac{1}{2}\phi^2\left(-A + \frac{B}{2}\phi^2\right) + \frac{\kappa}{2}(\nabla\phi \cdot \nabla\phi)\right] \mathrm{d}V \tag{13}$$

The first term provides an ideal gas equation of state, the second term is a double-well potential that causes phase separation at minima with compositions of $\phi_0 = \pm\sqrt{\frac{A}{B}}$, and the third term creates interfacial energy by associating energy with changes in ϕ. The parameters A and B specify the shape of the double-well potential. To have two phases with $\phi_0 = \pm 1$, we use $A = B$. The magnitude of the energy due to concentration gradients is determined by the parameter κ. The chemical potential for this free energy is

$$\mu = \frac{\delta F}{\delta \phi} = -A\phi + B\phi^3 - \kappa \nabla^2 \phi \tag{14}$$

The one-dimensional steady-state solution for ϕ between two infinite domains provides important information about the interface, specifically its characteristic thickness and excess energy. The solution is[23]

$$\phi(x) = \phi_0 \tanh \frac{x}{\zeta} \tag{15}$$

The length scale $\zeta = \sqrt{\frac{2\kappa}{A}}$ characterizes the thickness of this diffuse interface. Though 96.4% of the total change in ϕ across an interface occurs over a distance 4ζ, the length ζ is often called the interface thickness. The excess interfacial energy of this interface profile is

$$\sigma = \frac{2\sqrt{2}}{3}\sqrt{\kappa A} \tag{16}$$

For the large droplet sizes that are used in this work ($R > 20$ lattice nodes), the interfacial energy for a planar interface provides a good estimate of the energy of a spherical interface.[26]

In this first detailed characterization of the coalescence of droplets in LBM simulations, we keep several parameters constant and leave studying their effects as future work. To minimize spurious currents and enhance stability, we keep the two relaxation rates fixed ($\tau_f = \tau_g = 1$). Consequently, $\nu = \frac{1}{6}$ and $M = \frac{\Gamma}{2}$. The Reynolds number is fixed at one, and we consider pairs of fluids with equal densities and viscosities. In earlier work,[52] the critical capillary number for film rupture was found to be independent of the Reynolds number over the range $0.2 < \mathrm{Re} < 1.4$ in simulations with $R = 25$.

To maximize the droplet size that can be simulated with available computational resources, we take advantage of the symmetry in the full domain and simulate only one quarter of it. As shown in Fig. 1, the quarter-domain has two periodic boundaries, two symmetry boundaries, a rotational symmetry condition at the bottom ($y = \frac{1}{2}H$), and a shear plane on top ($y = H$). The shear velocity condition $\vec{u}|_{y=H} = (u_0, 0, 0)$ on this plane was implemented using the method of Ladd[53]. This method was chosen because it ensures mass conservation (unlike e.g. the method of Zou and He[54]), an important feature for the long simulation times that are used to study droplet collisions.

The central results of this paper are the effects of the parameters in the free-energy model on

the outcome of a simulated droplet collision. The model provides a convenient choice for the characteristic length l_c: the characteristic length ζ of the diffuse interface thickness. The Péclet number

$$\mathrm{Pe} = \frac{\dot{\gamma} R \zeta}{MA} \tag{17}$$

is the ratio of the time scales of advection and chemical potential diffusion over a length scale given by ζ.[24] Using $l_c = \zeta$ and including the Péclet number, we write

$$\mathrm{Ca}_c = \mathrm{Ca}_c \left(\mathrm{Re}, \frac{\Delta X}{2R}, \frac{\Delta Y}{2R}, \frac{2R}{H}, \frac{R}{\zeta}, \mathrm{Pe} \right) \tag{18}$$

We study the effects of the droplet size relative to the interface thickness $\frac{R}{\zeta}$, the interface Péclet number Pe, the confinement $\frac{2R}{H}$, and the vertical offset $\frac{\Delta Y}{2R}$ on Ca_c at constant Re and $\frac{\Delta X}{2R}$ to determine whether free-energy LBM simulations can be used to accurately model the physical problem. Other numerical factors that may affect the results, such as the relaxation rate, are kept constant. We study a parameter range in which the effects of the parameters on the critical capillary number can be determined with the computational resources that are currently available to us. We hypothesize that the model parameter ζ can be related to a physical l_c so that the simulations represent the physical situation when $\frac{R}{\zeta}$ and $\frac{R}{l_c}$ are matched. If this is correct, the effective physical size of the simulated droplets can be determined from the experimental size of a droplet system with the same Ca_c, Re, and geometry.

Implementation

A highly-parallel code was used to simulate the large domains that are required to discern the effects of the parameters on the outcome of a collision. The smallest ($R = 25$ lattice nodes) simulations were performed on a single graphics processing unit (GPU). The largest ($R = 100$ lattice nodes) simulations were parallelized over nine GPUs (NVIDIA Tesla M2070), with three GPUs per computational node. For these multi-GPU simulations, only one CPU core (Intel Xeon E5649) was used on each node for communication. This communication was implemented with a Mes-

sage Passing Interface (MPI) library. Sample performance data for the simulations are listed in Table 1. All computations were performed with double (64 bit) precision. The memory bandwidth that is shown is an effective bandwidth that includes only memory transfers that are required by the LBM calculations; memory transfers for communication are excluded. The speed is measured in million lattice updates per second (Mlups). For the largest domain size, 232 Mlups is approximately 300000 timesteps per day. The corresponding non-dimensional strain for 300000 timesteps at Re $= 1$ and $R = 100$ is $\dot{\gamma}t = 5$.

Table 1: Performance of the simulation software with different domain sizes and types of parallelization

Nodes	GPUs	Domain Size (lattice nodes)	Drop Radius, R (lattice nodes)	GPU Memory (GB)	Bandwidth (GB/s)	Speed (Mlups)
1	1	$256 \times 64 \times 64$	25	0.5	75	40.8
1	3	$256 \times 64 \times 64$	25	0.5	132	72.8
3	9	$1024 \times 256 \times 256$	100	34	426	232

Results and discussion

Many parameters remain constant for all the simulations that are presented in this section, unless specified otherwise. These parameters are: Re $= 1$, $\zeta = 2$, Pe $= 10$, $\frac{\Delta X}{2R} = 1.26$, $\frac{\Delta Y}{2R} = 0.86$, and $\frac{2R}{H} = 0.39$.

Interface resolution

Before studying the conditions that determine when colliding droplets coalesce, we first examine whether the simulation results are sensitive to the resolution of the interface and the size of the periodic domain. To determine if the interface is adequately resolved with $\zeta = 2$, simulations with twice this resolution were also performed. As illustrated in the upper portion of Fig. 2, the transition from $\phi = -1$ to $\phi = 1$ occurs over a distance of about 8 nodes when the characteristic length ζ of the diffuse interface is 2. With $\zeta = 4$, the distance is 16 nodes. Since the higher-

resolution interface profile is effectively identical to the lower-resolution profile, the interface is judged to be well-resolved at the lower resolution.

Three capillary numbers were considered to see the effect of the interface resolution on the outcome of a collision. All the simulations, shown in Fig. 2, were performed with the same geometry, Reynolds number (1), Péclet number (10), and $R/\zeta = 18.75$. The simulation at the lower resolution had a droplet radius of 37.5, a domain size of $384 \times 96 \times 96$, and an interface thickness of $\zeta = 2$; the simulation with $R = 75$ was in a $768 \times 192 \times 192$ domain and had $\zeta = 4$. At both resolutions, the transition from coalescence to sliding occurs over the range of capillary numbers from 0.08 to 0.1. At the higher resolution and $\mathrm{Ca} = 0.09$, a bridge between the two drops is visible in the fourth frame of the sequence in Fig. 2. Such a bridge also forms and breaks at the lower resolution, but it breaks sooner and is not visible in the frames chosen for Fig. 2. These results show that doubling the resolution does not change the critical capillary number significantly. As will be described in "Droplet size effect," keeping the interface thickness constant at $\zeta = 2$ in simulations with $R = 37.5$ and $R = 75$ lowers the critical capillary number by almost a factor of three. Due to the absence of a significant change in the critical capillary number when doubling the resolution, the interface is judged to be adequately resolved with $\zeta = 2$. This choice for ζ agrees with the findings of van der Graaf and van der Sman,[24,25] who used this interface thickness because it provided the correct critical capillary number for droplet breakup in a shear flow. They found that the critical capillary number for breakup was too low with $\zeta = 1$. Since $\zeta = 2$ provides adequate resolution, all further simulations were performed with this interface thickness. This choice allows us to simulate larger droplet sizes relative to the interface thickness with less computational resources.

Domain size effect

Since the simulated domain is periodic in the two directions that are perpendicular to the height of the domain (i.e. the x and z axes in Fig. 1), we evaluated the effect of the domain size in these directions. The results for two domain sizes with $R = 37.5$ and $\mathrm{Ca} = 0.08$, 0.09, and 0.10 were compared. The larger domain was $768 \times 192 \times 384$, which has twice the length and width of the

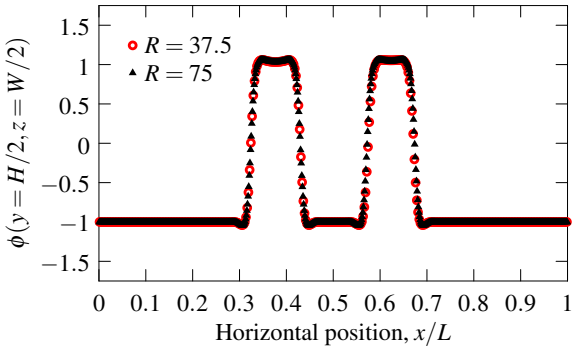

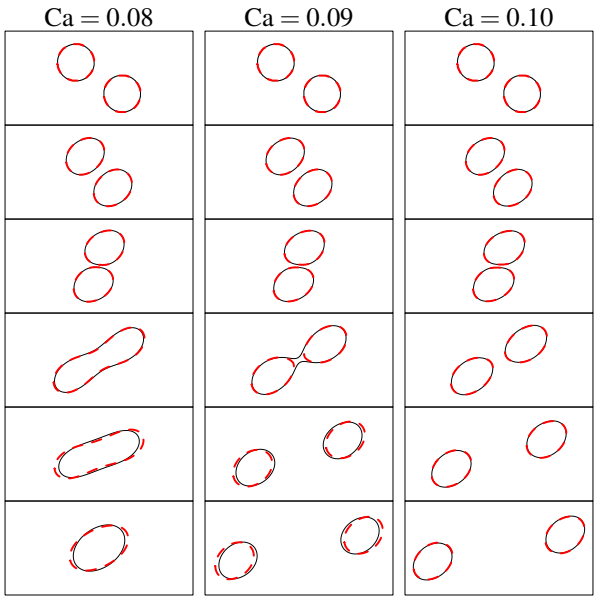

Figure 2: Effect of resolution on droplet collision simulations. The upper portion shows the value of ϕ along the x direction through the middle of the domain. Profiles are shown for the two resolutions ($R = 37.5$ and 75) at an early time when a smooth profile has been established but before significant shear has occurred ($\dot{\gamma}t = 0.13$). The profiles were visually identical for the three capillary numbers considered in the lower portion. The lower portion shows time series of the interface shape in cross-sections through the middle of the domain with $R = 37.5$ (dashed red) and $R = 75$ (solid black) at Ca $= 0.08$ (left), 0.09 (middle), and 0.1 (right). Time progresses from top ($\dot{\gamma}t = 0$) to bottom ($\dot{\gamma}t = 6.67$) in increments of $\dot{\gamma}t = 1.33$.

smaller $384 \times 192 \times 192$ domain. Doubling these two dimensions did not change the shape of the droplets or the outcome of a collision at the three capillary numbers. A domain with $L \approx 10R$ and $W \approx 5R$ is therefore large enough that the effects of periodicity are minor. However, the effect of confinement, which is the ratio of the domain height and droplet diameter, is important, and this effect is discussed in the section "Confinement effect."

Droplet size effect

The effect of the droplet size on the outcome of a collision was studied by increasing the droplet radius and domain size in proportion while keeping the interface thickness (ζ, expressed as a number of lattice nodes) constant. This is in contrast to the simulations used to study the effects of the interface resolution (Fig. 2) in which the interface thickness was also scaled up by the same factor as the droplet radius and domain size. In the simulations used to study the effect of the droplet size, the Reynolds number, Péclet number, and geometry were kept constant at the previously-listed values. The simulations with different droplet sizes but the same interface thickness represent the physical situation of studying collisions of differently-sized droplets of the same pair of liquids. When the same liquid pair is used, the intermolecular interactions that determine the critical film thickness remain constant.

Figure 3 shows how the capillary number and the size of the droplet relative to the interface thickness determine the outcome of a collision. A bisection search method was used to find the critical values when the transitions between different outcomes occur. In general, droplets slide unless the capillary number is below a critical value. This critical capillary number decreases as the droplet becomes larger relative to the interface thickness, or equivalently, the interface thickness becomes smaller relative to the droplet radius. Considering previous discussion, this decreasing trend occurs because reducing the critical thickness for film rupture delays coalescence by increasing the time required for the film to drain. If the observed decreasing trend in the critical capillary number with increasing droplet size continues beyond the parameter range we studied, it is expected that droplets will not coalesce in the limit of a sharp interface, i.e. as $R/\zeta \to \infty$. Thus, to

simulate a physical system in which droplets coalesce, a finite $\frac{R}{\zeta}$ value is required.

As illustrated in Fig. 3, there are three possible outcomes of a simulated droplet collision for the parameter ranges that we consider. For every droplet size, there is a critical capillary number above which the droplets slide over each other and their interfaces remain distinct. There is also a critical capillary number below which the droplets coalesce. These two critical capillary numbers, however, are not necessarily the same.

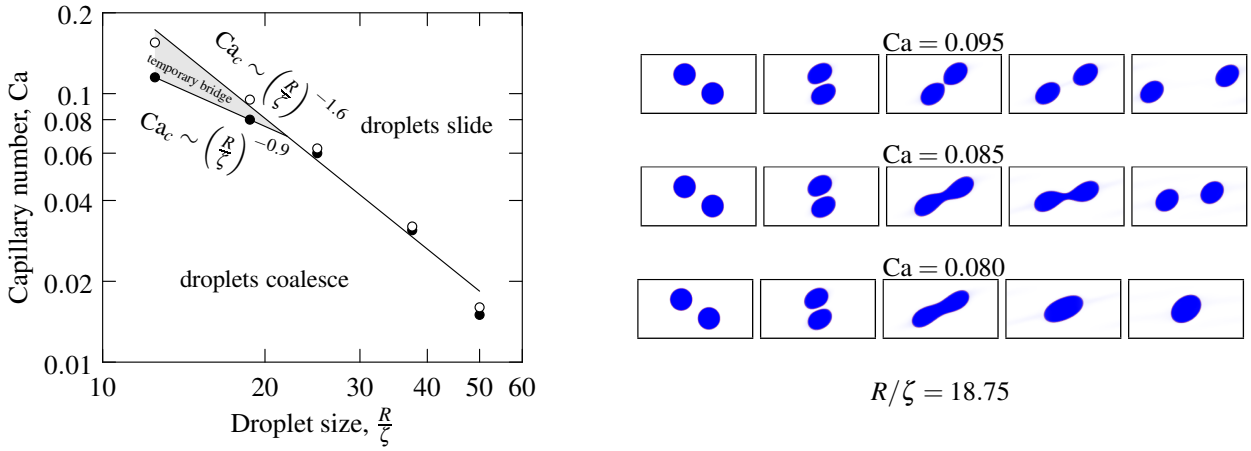

Figure 3: The effect of the droplet size (left) on the critical capillary numbers that separate the three possibilities (right) for the outcome of a simulated droplet collision. The open circles show the simulations with the lowest capillary number for a given droplet radius at which the two droplets remained separate. The filled circles show the highest capillary number at which the droplets coalesce. Solid lines show fitted scaling laws. The time sequences on the right show sample collisions with $R/\zeta = 18.75$ in which the droplets slide (top), a temporary bridge forms (middle), and the droplets coalesce (bottom). Cross-sections of the ϕ field are shown in the x-y plane through the middle of the domain with colours ranging from white ($\phi = -1$) to blue ($\phi = 1$). The $\phi = 0$ contour is shown in red. Animations are included as online supplementary information.

The effect of the droplet size relative to the interface thickness $\left(\frac{R}{\zeta}\right)$ on the two critical capillary numbers is shown in Fig. 3. When $\frac{R}{\zeta} > 22$, there is only one critical capillary number that separates the regions of sliding and coalescence. When $\frac{R}{\zeta} < 22$ the situation is more complex. The higher critical capillary number specifies when the interfaces come close enough for the film to rupture. The newly-formed bridge is pulled apart by the shear flow. This happens until the capillary number falls below the lower critical capillary number that specifies when the outcome of a collision is coalescence. Both critical capillary numbers follow a simple scaling rule $\mathrm{Ca}_c \sim \left(\frac{R}{\zeta}\right)^{-n}$ with

different values of n (with $n > 0$). Since n for the lower Ca_c is smaller than n for the higher Ca_c, the two capillary numbers eventually become the same, and then the critical capillary number for film rupture becomes the critical value that determines if drops coalesce. This result is consistent with experiments[13] in which only one critical Ca for coalescence was observed. This suggests that the droplets in the experiments are sufficiently large that only one Ca_c exists. Experiments with smaller droplets are not available to verify if temporary bridges would be observed with smaller droplets.

To interpret the existence of a temporary bridge in simulations, we can compare the characteristic time scales of shear and bridge growth. The shear time scale is $\tau_s = \dot{\gamma}^{-1}$. The growth of the liquid bridge between drops is a complex phenomenon and only a brief discussion is presented here. There are two regimes for the growth of the bridge radius R_b over time (see e.g. Paulsen et al.[55]): a viscous and an inertial regime. Fig. 4 shows the growth of the bridge as a function of time for a simulation with $R = 37.5$, $\zeta = 2$, and $\frac{\sigma R}{\rho v^2} = 10.8$. The bridge radius R_b is proportional to the square root of time scaled by the inertial time scale $\tau_i = \sqrt{\frac{\rho R^3}{\sigma}}$, indicating that our binary-liquid simulations, like the liquid-vapour simulations by Lee and Fischer,[56] are consistent with modelling for the inertial regime.[57] The proportionality factor of 0.7, however, is lower than the 1.2 found by Lee and Fischer.[56] An important difference between the modelling discussed here and the liquid-liquid coalescence experiments and simulations is that the modelling considers liquid drops in a vapour whose effects are often neglected. The slower growth of the bridge in liquid-liquid simulations may be due to the increased inertia of a liquid film compared to a lower-density vapour film. Having shown that the inertial time scale determines the rate of bridge growth in the simulations, we can consider the ratio of the shear and inertial bridge growth time scales

$$\frac{\tau_s}{\tau_i} = \frac{\dot{\gamma}^{-1}}{\sqrt{\frac{\rho R^3}{\sigma}}} = \frac{1}{\sqrt{\mathrm{ReCa}}} \tag{19}$$

to determine the outcome of the competition between growth and shear that starts when the film ruptures and the bridge forms. When $\tau_s/\tau_i \ll 1$, the shear time scale is smaller than the bridge

growth time scale, and we expect the slowly-growing bridge to be pulled apart; when $\tau_s/\tau_i \gg 1$, the bridge grows faster than shear pulls it apart, allowing the droplets to coalesce. A critical value of the ratio τ_s/τ_i must be exceeded for the droplets to coalesce. The value of this critical ratio may depend on various parameters. Based on the lower Ca_c values in Fig. 3, the critical value of τ_s/τ_i for the conditions of these simulations is slightly higher than 3. If this critical time scale ratio remains constant, the critical capillary number for bridge destruction scales as $\mathrm{Ca}_c \sim \mathrm{Re}^{-1}$ based on Eq. 19. At low Re, the dynamics switch to a viscous regime, and the Re^{-1} scaling is not applicable (by using the viscous time scale $\tau_v = \frac{\mu R}{\sigma}$ instead of τ_i, the time scale ratio Eq. 19 becomes the inverse of the capillary number and is therefore independent of Re). Thus in addition to the difference in droplet size relative to intermolecular length scales, the absence of experimental observations of a regime where a bridge forms and breaks may be also due to the difference in Reynolds numbers: the experiments of Chen et al.[13] had $\mathrm{Re} < 1 \times 10^{-7}$ compared with $\mathrm{Re} = 1$ in the simulations.

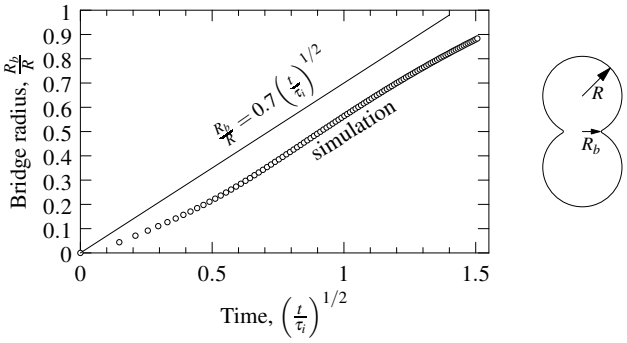

Figure 4: The radius of the bridge between two initially separate droplets in a simulation, which is illustrated on the right, grows with the square root of time scaled by the inertial time scale τ_i. The solid line shows the slope estimated at $t = \tau_i$.

Interface diffusivity effect

The chemical potential diffusivity, or mobility M (defined in Eq. 12), affects the critical capillary number for coalescence. Qualitatively, if the diffusivity is low, the ϕ profile over an interface responds slowly to changes in local conditions. As diffusion speeds up compared to advection, the interaction time between two interfaces that is required for sufficient diffusion to cause film

rupture decreases. The critical capillary number increases, i.e. coalescence becomes "easier," as the mobility increases (Pe decreases).

Previous studies of the effect of the interface diffusivity in multiphase flow simulations with the free-energy method have not considered coalescence. Van der Graaf et al.[24] performed three-dimensional simulations of droplet formation in a microfluidic T-junction. They verified that the critical capillary number for droplet breakup in a simple shear flow was correct for their choice of resolution and Péclet number. Van der Sman and van der Graaf[25] systematically studied droplet deformation and breakup in two-dimensional simulations with the free-energy method. Yue and Feng[58] discuss diffuse-interface modelling of contact line motion on solid surfaces, a problem with features that are relevant to simulations of coalescence. In the limit of a sharp interface (a non-diffusing interface with zero thickness), contact lines remain unphysically pinned. The sharp-interface limit is also unphysical for simulations of coalescence. Reducing the interface thickness relative to the droplet size delays coalescence because the thickness of the film between the drops must thin to a greater extent before coalescence, as was shown in the section "Droplet size effect". Zero diffusivity is also undesirable because, in the absence of diffusivity, adjacent interfaces would not merge to cause coalescence. In simulations of contact line motion, the limit of zero thickness and non-zero diffusivity is desired,[58] while both a non-zero interface thickness and diffusivity (and therefore a finite Péclet number) are required for coalescence. In fact, van der Sman and van der Graaf[25] found that the critical capillary number for droplet breakup in shear is correct when the rates of interface advection and diffusion balance, i.e. the Péclet number is near one. In three-dimensional simulations, van der Graaf et al.[24] obtained the correct critical capillary number for breakup in shear with $\mathrm{Pe} = 10$. Droplet breakup and coalescence, however, involve topologically and hydrodynamically different interactions between two interfaces. As a result, the correct choice of the Péclet number for simulations of breakup and coalescence may not be the same. We therefore study the effect of the Péclet number on coalescence in this section. In the other sections, $\mathrm{Pe} = 10$ was used.

The effect of the Péclet number on the collision outcome map (Fig. 3) is shown in Fig. 5. All

dimensionless parameters were kept constant except the interface Péclet number that was varied between 1 and 100. Numerical instability prevented simulations with Pe $= 100$ and $R/\zeta > 25$. In general, as the Péclet number decreases, the critical capillary numbers increase and the area of the region where temporary bridges form increases. The critical capillary numbers as a function of the Péclet number for $R/\zeta = 18.75$ are also shown in Fig. 5. As expected, increasing the Péclet number lowers Ca_c. Compared to the effect of R/ζ on Ca_c, the effect of the Péclet number is weaker: Ca_c decreases by a factor of four as the Péclet number increases by a factor of 100, while doubling R/ζ reduces Ca_c by a factor of three. In the advection dominated region with Pe > 50, a temporary bridge does not form, and both Ca_c values become constant at about 0.05. As the Péclet number decreases, both critical capillary numbers increase and the difference between them also increases. If both breakup and coalescence can be simulated correctly with the same Péclet number, the results with Pe $= 10$ (with which van der Graaf et al.[24] obtained breakup at the correct capillary number) may be considered predictive. A region of temporary bridge formation is thus expected to exist in experiments, but experimental evidence is not presently available to assess this prediction. The existence and size of the parameter range for temporary bridge formation is highly sensitive to the Péclet number.

Offset effect

To study the effect of the vertical offset, we performed additional simulations with a lower offset ΔY between the droplets. Simulations with capillary numbers exceeding 0.2 were not performed because the deformation of the droplets became significant, and the periodicity of the domain began to influence the outcome of the simulations. The non-dimensional vertical offset for the second set of simulations was 0.6. All other parameters were kept constant. The results of these simulations are compared with the previous simulations with an offset of 0.86 in Fig. 6. As the vertical offset decreases, the geometry approaches that of a head-on collision, and the Ca_c for coalescence increases. Simulations with $R = 100$ were also performed at $\frac{\Delta Y}{2R} = 0.3$ and 0.4. Results for $\frac{\Delta Y}{2R} = 0.4$ are shown in Fig. 7. At these offsets, critical capillary numbers between 0.1 and 0.25

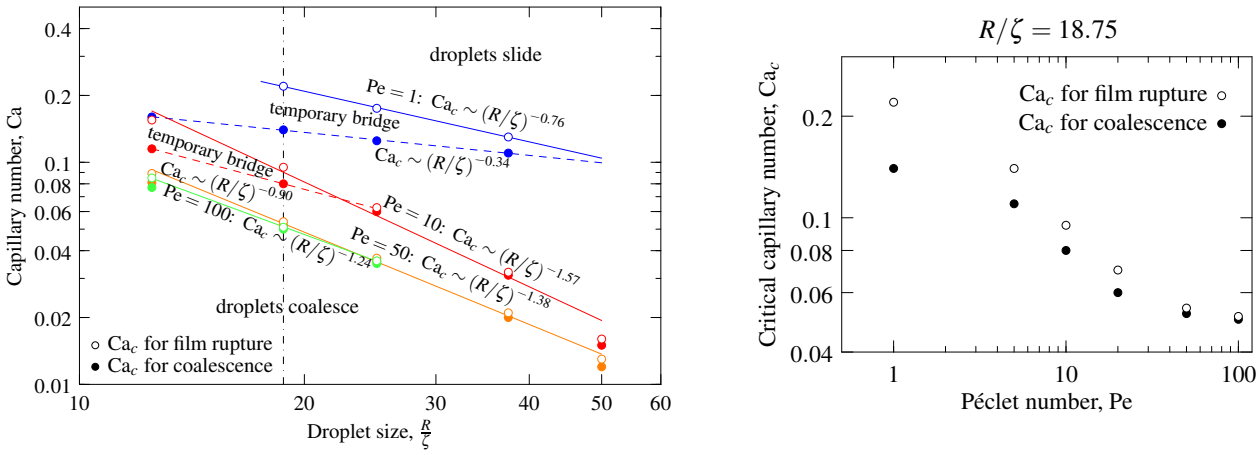

Figure 5: Effect of the Péclet number on the collision outcome map (left). The results for Péclet numbers of 1 (blue), 10 (red), 50 (orange) and 100 (green) are shown. The solid and dashed lines show fitted scaling laws. The dashed lines are for the high Ca at which the droplets remain coalesced; the solid lines are for the lowest Ca at which the droplets slide. At capillary numbers between these lines, a bridge forms then breaks. The effect of the Péclet number on the two critical capillary numbers at a constant droplet size of $R/\zeta = 18.75$, indicated by the vertical dash-dotted line on the left, is shown on the right.

are expected. Precise values were not obtained due to the computational requirements of the large domains. At these lower offsets, the droplets switch to coalescing in the compression stage (i.e. before sliding over each other) rather than the extension stage (when they move apart after sliding over). Comparing Figs. 3 and 7, the change in the critical capillary numbers and the relative orientation at coalescence (compression versus extension) can be seen. Complex behaviour is seen at $\mathrm{Ca} = 0.15$. An internal droplet is present in the bridge and multiple drops form when the bridge breaks. Simulations at low offsets will be studied in greater detail in the future. Significantly larger droplets (and therefore simulation domains) are needed to determine the critical capillary number at the vertical offset of 0.16 for the droplets in the experiments of Chen et al.[13]

Confinement effect

The effect of confinement was studied using simulations with the same range of radii as previously but in a domain with a constant size. In Fig. 8, the results of these simulations with a fixed domain size of $1024 \times 256 \times 256$ are compared to the previous simulations that had a constant confinement.

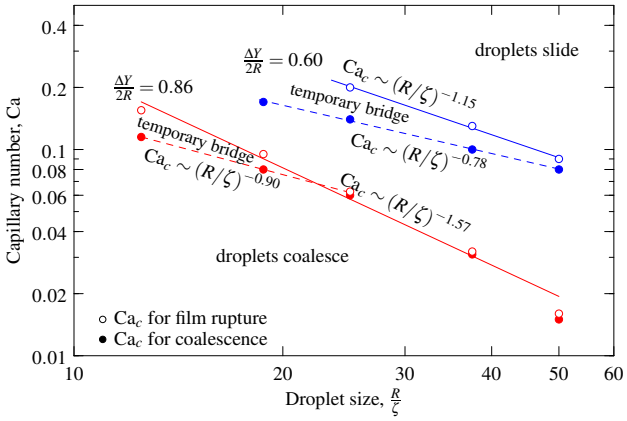

Figure 6: Effect of the vertical offset on the critical capillary numbers for coalescence. The red lines are for an offset of 0.86; the blue lines are for 0.60. A temporary bridge forms for capillary numbers between the open and filled symbols.

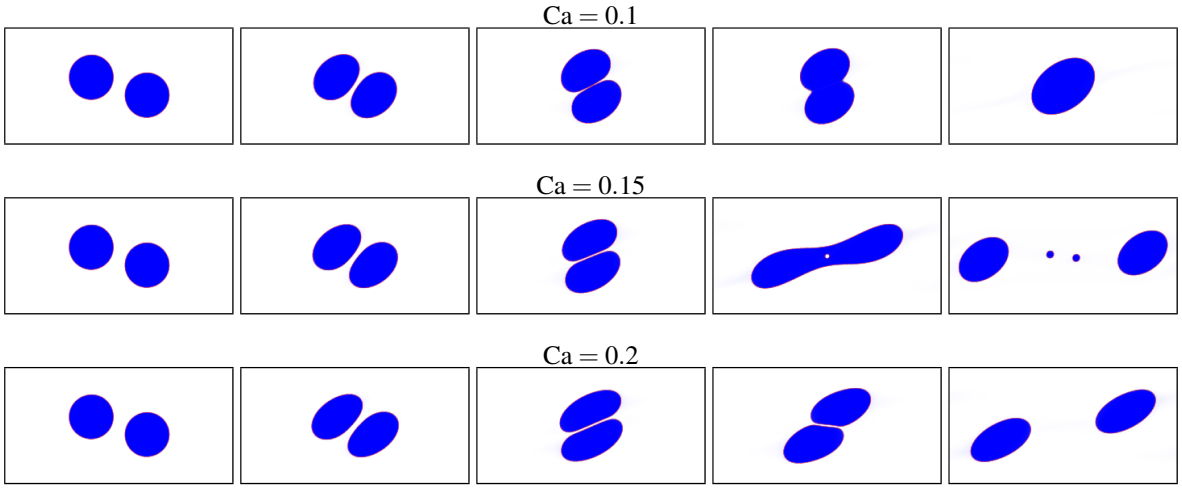

Figure 7: Sample collisions between droplets with $\frac{\Delta Y}{2R} = 0.4$ and $\frac{R}{\zeta} = 50$. The time increments are not uniform, differ between the three cases, and were chosen to illustrate the different stages of the collisions well.

Numerical instability prevented the completion of simulations at $\frac{2R}{H} = 0.29$ with Ca < 0.008. The critical capillary number is therefore not known for this confinement, but must be below 0.008. The open circle indicates this lowest capillary number that could be simulated. Comparing with the constant high-confinement $\left(\frac{2R}{H} = 0.39\right)$ simulations, reducing the confinement first decreases the critical capillary numbers, then increases them until they eventually exceed those for the highly-confined case. The reason for the reduction in the critical capillary numbers at $\frac{R}{\zeta} = 25$ is illustrated in Fig. 8. In the larger domain, the droplets are more free to move vertically and slide over each other. As a result, a lower shear rate (and therefore Ca) is needed to prevent sliding and cause coalescence.

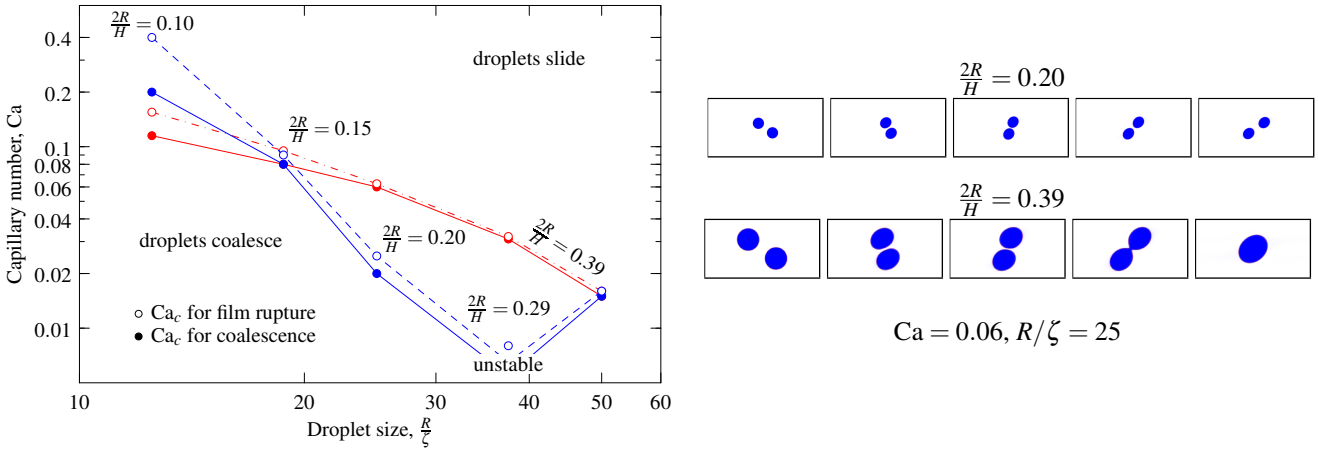

Figure 8: (left) Effect of confinement on the critical capillary numbers for coalescence. The red lines are for a constant confinement $\frac{2R}{H} = 0.39$. The blue lines are for a constant domain size and varying droplet sizes (and therefore confinements). (right) Sample collisions between droplets with confinements of $\frac{2R}{H} = 0.20$ (top) and 0.39 (bottom) and the same capillary number (Ca $= 0.06$) and droplet size ($R/\zeta = 25$). The images have been scaled so that the domains are the same size; the domain for $\frac{2R}{H} = 0.20$ is double the size of the domain for $\frac{2R}{H} = 0.39$.

Comparison with Experimental Results

While detailed experimental results are available for droplet coalescence in the extensional flow of a four-roll mill,[9–12] few experimental results are available for simple shear flow. Early work by Guido and Simeone[8] did not determine critical capillary numbers. Recently, Chen et al.[13]

reported critical capillary number ranges for confined and unconfined droplets in simple shear. Though these results are the most relevant to our simulations, they cannot be compared quantitatively. Considering the increasing trend in the critical capillary number with decreasing droplet size, the high critical values for the simulations indicate that the effective physical sizes of the simulated droplets are smaller than those used in the experiments (radii 50 to 150 μm). Furthermore, the vertical offsets produced by breaking a drop are lower (0.16) than the lowest offset for which critical capillary numbers could be estimated in the simulations (0.3). Chen et al. [13] also present results for effectively unconfined droplets and droplets with varying confinement, while simulations with constant high confinement are most practical to obtain from simulations. Finally, the small difference in horizontal offset likely has a minor effect, while the difference in Reynolds number (1 in simulations vs. 10^{-7} in experiments) may be important. This Reynolds number is based on the droplet radius, and a Reynolds number based on the film thickness would be one to two orders of magnitude smaller in the simulations. The flow in the draining film is therefore likely in the Stokes regime for both the simulations and experiments. Due to the differences in the parameters between the simulations and experiments, we can only compare the results qualitatively. The simulation results are nonetheless useful because they indicate how different numerical parameters affect the critical capillary number and therefore how experiments and simulations can be matched by choosing the parameters correctly.

One key difference between the simulations and the experiments of Chen et al. [13] is the stage of the collision process in which coalescence occurs. Chen et al. obtained critical capillary numbers between 0.001 and 0.008 and always saw coalescence during the compression stage of the collision when the shear flow pushes the droplets together. In contrast, Guido and Simeone [8] observed coalescence during extension at $\mathrm{Ca} = 0.13$, but with a viscosity ratio of 0.36 (droplet phase over continuous phase; the ratio is 1.1 for the experiments by Chen et al. [13] and 1 in the LBM simulations). The coalescence of droplets in the extension stage of the simulations is likely due to the high capillary numbers at which the droplets coalesce and the large vertical offset.

To understand the differences in fluid and interface parameters between the experiments and

simulations better, we re-visit the bridge growth phenomenon. By differentiating the equation describing the growth rate of the bridge, $\frac{R_b}{R} = 0.7\left(t\sqrt{\frac{\sigma}{\rho R^3}}\right)^{1/2}$, a Reynolds number Re_b that characterizes the speed of the interface can be defined. Taking the growth rate of the bridge radius R_b at time $t = \tau_i$ as the characteristic speed and the droplet radius as the characteristic length, this Reynolds number is

$$\mathrm{Re}_b \equiv \frac{R}{\nu}\left.\frac{\mathrm{d}R_b}{\mathrm{d}t}\right|_{t=\tau_i} = \frac{1}{2}\sqrt{\frac{\sigma R}{\rho \nu^2}} \tag{20}$$

The proportionality factor of order one has been omitted. In the limit of high Re_b, the momentum generated at the growing bridge cannot diffuse over the radius of the droplet in the time it takes the bridge to grow. If Re_b is low, momentum diffusion is fast, and the inertial growth model is invalid. This Reynolds number is related to the non-dimensional quantity $\frac{\sigma R}{\rho \nu^2}$, called the Suratman number Su.[59] With this definition of Su, $\mathrm{Re}_b = \frac{1}{2}\sqrt{\mathrm{Su}}$. For the shear flow simulations, $\mathrm{Su} = \frac{\mathrm{Re}}{\mathrm{Ca}}$ and is between 5 and 100. In contrast, $\frac{\sigma R}{\rho \nu^2} \approx 10^{-6}$ for the experiments by Chen et al.[13] due to the high viscosity of the polymers they used. The growth of bridges between their polymer droplets is therefore not in the inertial regime, but rather in the viscous regime. If experiments are possible with a fluid pair that has a viscosity similar to water, the results could be compared with the simulations. Using $\sigma = 2$ mN/m, $\rho = 1000$ kg/m^3, $R = 10$ μm, and $\nu = 10^{-6}$ m^2/s, the value of $\frac{\sigma R}{\rho \nu^2}$ is 20, which is within the range that is feasible for simulations. While the difference in Suratman number between the experiments and simulations clearly affects the post-coalescence growth of the bridge, its effect on the pre-coalescence shape and trajectory of the droplets remains to be studied in greater detail.

In both experiments and simulations, the critical capillary number decreases as the droplet size increases. Due to the differences in parameters between the simulations and experiments, comparing the rate of the decrease is difficult. For reference, the experimental data of Chen et al.[13] for unconfined droplets are provided in Fig. 9. The experimental data do not follow a simple power law scaling, but the slope for simulations with $\mathrm{Pe} = 10$ is shown for comparison. The exponent was determined for simulations at a constant confinement of 0.39, while the experimental results are for unconfined droplets ($2R/H < 0.1$). Considering Figs. 5 and 8, the rate of decrease is higher for

low confinement and increases with increasing Péclet number. The apparent agreement between the exponent for unconfined experimental droplets and the confined droplet simulations at $\mathrm{Pe} = 10$ is likely coincidental. Further experiments or simulations at matching parameters are required to evaluate the results. Due to the effect of the Péclet number on the exponent in the scaling law, the correct Péclet number for simulations could be determined by matching the exponent to experimental data.

It is worth noting that experimental results and scaling laws for the effect of the droplet size on the capillary number are presented by showing the capillary number (a dimensionless quantity) as a function of the droplet radius (a dimensional quantity).[9–13] Ideally, one would non-dimensionalize the droplet size by an appropriate physical length scale, but the correct choice is not clear. If simulations and experiments with equal values for all dimensionless parameters were feasible, it would be possible to determine the effective physical length that corresponds to the interface thickness ζ in simulations. This length, however, would likely not be universal and would depend on the specific liquid pair being considered.

As the vertical offset is decreased from 0.86 to 0.3 in the simulations, the critical capillary numbers increase by about one order of magnitude. The collision stage in which the droplets coalesce changes from being the extension stage at high offsets to the compression stage at low offsets. Coalescence during compression at low offsets and extension at high offsets is qualitatively consistent with the observations of Yoon et al.[12] for extensional flows.

The trend in the critical capillary numbers for constant domain size qualitatively matches the experimental results of Chen et al.[13]. Chen et al. found that the critical capillary number decreases monotonically as the droplet size increases in a fixed domain height when the confinement is low (< 0.2). The critical capillary number then rises once the confinement exceeds 0.2. In the simulations, a decrease in the critical capillary number was seen until a confinement of about 0.3, after which the critical capillary number increases.

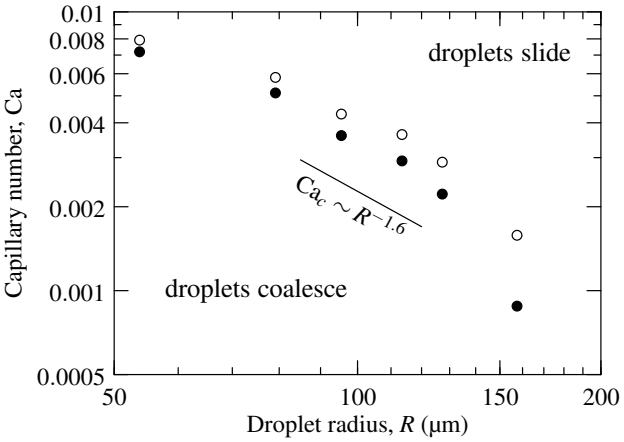

Figure 9: Experimental data of Chen et al.[13] for unconfined droplets in simple shear flow. The open symbols show the lowest capillary number at which the droplets slide; the filled symbols show the highest capillary number at which they coalesce.

Conclusions

Highly-resolved, three-dimensional simulations of equal-size liquid droplets colliding in the simple shear flow of another liquid were performed using the free-energy lattice Boltzmann method. In such a shear flow, the droplets coalesce unless a critical capillary number is exceeded. While the droplets in previous simulations were too small to determine the critical capillary number, we used a highly-parallel code to simulate sufficiently large domains. With these large-scale simulations, we determined the critical capillary number and explained why droplets coalesced at unrealistically high capillary numbers in previous simulations. The most important factor that determines the critical capillary number in the simulations is the relative size of the droplets with respect to the thickness of the diffuse interface. The critical capillary number decreases as the size of the droplets increases. When the droplet radius is 25 lattice nodes and the characteristic thickness of the interface is 2, which are typical values for droplet simulations, the critical capillary number is 0.16. Our largest simulations had droplets with radii of 100 lattice nodes; with these large droplets, the critical capillary number was 0.016. The interface diffusivity, expressed as a Péclet number, also affects the critical capillary number. With faster diffusion (lower Péclet number), droplets coalesce at higher capillary numbers. A parameter range was found where small droplets temporarily coalesce until shear pulls the newly-formed droplet apart. Two geometric parameters, the

vertical offset and confinement, were also considered. As the vertical offset between the droplets is decreased, the critical capillary number increases and the time of coalescence switches from the extension stage to the compression stage of the collision. If the domain size is kept constant and the droplet size is increased (thereby increasing the confinement), the critical capillary number first decreases then increases, as in experiments.

The results of the simulations appear to be physically reasonable. However, simulations at the scale required to match experimental work reported in the literature remain computationally impractical. If experiments were instead performed with smaller droplets and less viscous fluids than the previously-used polymers, a direct comparison with simulations may now be possible due to the feasibility of sufficiently large-scale simulations. For such a direct comparison, we estimate that 1 to 50μm diameter droplets are required together with a fluid for which $\frac{\sigma R}{\rho \nu^2} \approx 20$. This value could be achieved with a fluid whose viscosity is approximately that of water. Such experiments are needed to determine the interface thickness and diffusivity (Péclet number) that should be used in simulations to correctly model physical systems. Experiments and simulations at matched conditions would also reveal the physical length scale that corresponds to the numerical interface thickness. Future work will involve simulations of larger droplets relative to the interface thickness and lower offsets to further explore the parameter space. The results presented in this paper are not only relevant to free-energy LBM simulations and likely also apply to simulations with other phase-field Cahn-Hilliard methods, such as those of Ceniceros et al.[60]

Acknowledgement

This research has been enabled by the use of computing resources provided by WestGrid and Compute/Calcul Canada. O.S. is supported by an Alexander Graham Bell Canada Graduate Scholarship from NSERC.

Supporting Information Available

Visualization movies of the droplet collision simulations at Pe $= 10$, $R/\zeta = 18.75$, and Ca $=$

0.08, 0.085, and 0.095 are included. They show the three outcomes of a collision. This material is available free of charge via the Internet at http://pubs.acs.org/.

References

(1) Tsouris, C.; Tavlarides, L. Breakage and Coalescence Models for Drops in Turbulent Dispersions. *AIChE Journal* **1994**, *40*, 395–406.

(2) Kostoglou, M.; Karabelas, A. A contribution towards prodicting the evolution of droplet size distribution in flowing dilute liquid/liquid dispersions. *Chem. Eng. Sci.* **2001**, *56*, 4283–4292.

(3) Laurenzi, F.; Coroneo, M.; Montante, G.; Paglianti, A.; Magelli, F. Experimental and computational analysis of immiscible liquid-liquid dispersions in stirred vessels. *Chem. Eng. Res. Des.* **2009**, *87*, 507–514.

(4) Teh, S.-Y.; Lin, R.; Hung, L.-H.; Lee, A. Droplet Microfluidics. *Lab Chip* **2008**, *8*, 198–220.

(5) Baroud, C.; Gallaire, F.; Dangla, R. Dynamics of microfluidic droplets. *Lab Chip* **2010**, *10*, 2032–2045.

(6) Bremond, N.; Bibette, J. Exploring emulsion science with microfluidics. *Soft Matter* **2012**, *8*, 10549–10559.

(7) Bremond, N.; Thiam, A.; Bibette, J. Decompressing Emulsion Droplets Favors Coalescence. *Phys. Rev. Lett.* **2008**, *100*, 024501.

(8) Guido, S.; Simeone, M. Binary collision of drops in simple shear flow by computer-assisted video optical microscopy. *J. Fluid Mech.* **1998**, *357*, 1–20.

(9) Hu, Y.; Pine, D.; Leal, L. Drop deformation, breakup, and coalescence with compatibilizer. *Phys. Fluids* **2000**, *12*, 484–489.

(10) Yang, H.; Park, C.; Hu, Y.; Leal, L. The coalescence of two equal-sized drops in a two-dimensional linear flow. *Phys. Fluids* **2001**, *13*, 1087–1106.

(11) Leal, L. Flow induced coalescence of drops in a viscous fluid. *Phys. Fluids* **2004**, *16*, 1833–1851.

(12) Yoon, Y.; Borrell, M.; Park, C.; Leal, L. Viscosity ratio effects on the coalescence of two equal-sized drops in a two-dimensional linear flow. *J. Fluid Mech.* **2005**, *525*, 355–379.

(13) Chen, D.; Cardinaels, R.; Moldenaers, P. Effect of confinement on droplet coalescence in shear flow. *Langmuir* **2009**, *25*, 12885–12893.

(14) Chesters, A. The modelling of coalescence processes in fluid-liquid dispersions: A review of current understanding. *Chem. Eng. Res. Des.* **1991**, *69*, 259–270.

(15) Cristini, V.; Tan, Y.-C. Theory and numerical simulation of droplet dynamics in complex flows — a review. *Lab Chip* **2004**, *4*, 257–264.

(16) Loewenberg, M.; Hinch, E. Collision of two deformable drops in shear flow. *J. Fluid Mech.* **1997**, *338*, 299–315.

(17) Zinchenko, A.; Davis, R. Shear flow of highly concentrated emulsions of deformable drops by numerical simulations. *J. Fluid Mech.* **2002**, *455*, 21–62.

(18) Zinchenko, A.; Davis, R. Large-scale simulations of concentrated emulsion flows. *Phil. Trans. R. Soc. Lond. A* **2003**, *361*, 813–845.

(19) Davis, R.; Zinchenko, A. Motion of deformable drops through granular media and other confined geometries. *J. Colloid Interf. Sci.* **2009**, *334*, 113–123.

(20) Tryggvason, G.; Scardovelli, R.; Zaleski, S. *Direct Numerical Simulations of Gas-Liquid Multiphase Flows*; Cambridge University Press, 2011; Chapter 10.

(21) Zaleski, S.; Li, J.; Succi, S. Two-Dimensional Navier-Stokes Simulation of Deformation and Breakup of Liquid Patches. *Phys. Rev. Lett.* **1995**, *72*, 244–247.

(22) Zhang, J. Lattice Boltzmann method for microfluidics: models and applications. *Microfluid Nanofluid* **2011**, *10*, 1–28.

(23) Briant, A.; Yeomans, J. Lattice Boltzmann simulations of contact line motion. II. Binary fluids. *Phys. Rev. E* **2004**, *69*, 031603.

(24) van der Graaf, S.; Nisisako, T.; Schroën, C.; van der Sman, R.; Boom, R. Lattice Boltzmann Simulations of Droplet Formation in a T-Shaped Microchannel. *Langmuir* **2006**, *22*, 4144–4152.

(25) van der Sman, R.; van der Graaf, S. Emulsion droplet deformation and breakup with lattice Boltzmann model. *Comput. Phys. Commun.* **2008**, *178*, 492–504.

(26) Jia, X.; McLaughlin, J. B.; Kontomaris, K. Lattice Boltzmann simulations of flows with fluid-fluid interfaces. *Asia-Pac. J. Chem. Eng.* **2008**, *3*, 124–143.

(27) Christopher, G.; Bergstein, J.; End, N.; Poon, M.; Nguyen, C.; Anna, S. Coalescence and splitting of confined droplets at microfluidic junctions. *Lab Chip* **2009**, *9*, 1102–1109.

(28) Chen, D. L.; Li, L.; Reyes, S.; Adamson, D.; Ismagilov, R. Using Three-Phase Flow of Immiscible Liquids to Prevent Coalescence of Droplets in Microfluidic Channels: Criteria to Identify the Third Liquid and Validation with Protein Crystallization. *Langmuir* **2007**, *23*, 2255–2260.

(29) Farhat, H.; Lee, J. Suppressing the coalescence in the multi-component lattice Boltzmann method. *Microfluid Nanofluid* **2010**, *11*, 137–143.

(30) Spencer, T.; Halliday, I.; Care, C. A local lattice Boltzmann method for multiple immiscible fluids and dense suspensions of drops. *Phil. Trans. R. Soc. Lond. A* **2011**, *369*, 2255–2263.

(31) Yue, P.; Feng, J.; Liu, C.; Shen, J. Diffuse-interface simulations of drop coalescence and retraction in viscoelastic fluids. *J. Non-Newtonian Fluid Mech.* **2005**, *129*, 163–176.

(32) Dupuy, P.; Fernandino, M.; Jakobsen, H.; Svendsen, H. Using Cahn-Hilliard mobility to simulate coalescence dynamics. *Computers and Mathematics with Applications* **2010**, *59*, 2246–2259.

(33) Premnath, K.; Abraham, J. Lattice Boltzmann simulations of drop-drop interactions in two-phase flows. *Int. J. Mod. Phys. C* **2005**, *16*, 25–44.

(34) Premnath, K.; Abraham, J. Simulations of binary drop collisions with a multiple-relaxation-time lattice-Boltzmann model. *Phys. Fluids* **2005**, *17*, 122105.

(35) Inamuro, T.; Ogata, T.; Tajima, S.; Konishi, N. A lattice Boltzmann method for incompressible two-phase flows with large density differences. *J. Comput. Phys.* **2004**, *198*, 628–644.

(36) Lee, T.; Lin, C.-L. A stable discretization of the lattice Boltzmann equation for simulation of incompressible two-phase flows at high density ratio. *J. Comput. Phys.* **2005**, *206*, 16–47.

(37) Sun, K.; Jia, M.; Wang, T. Numerical investigation of head-on droplet collision with lattice Boltzmann method. *Int. J. Heat and Mass Transfer* **2013**, *58*, 260–275.

(38) Chiappini, D.; Bella, G.; Succi, S.; Ubertini, S. Applications of finite-difference lattice Boltzmann method to breakup and coalescence in multiphase flows. *Int. J. Mod. Phys. C* **2009**, *20*, 1803–1816.

(39) Lycett-Brown, D.; Karlin, I.; Luo, K. Droplet collision simulation by a multi-speed lattice Boltzmann method. *Commun. Comput. Phys.* **2011**, *9*, 1219–1234.

(40) Shan, X.; Chen, H. Lattice Boltzmann model for simulating flows with multiple phases and components. *Physical Review E* **1993**, *47*, 1815–1820.

(41) Perlekar, P.; Biferale, L.; Sbragaglia, M.; Srivastava, S.; Toschi, F. Droplet size distribution in homogeneous isotropic turbulence. *Phys. Fluids* **2012**, *24*, 065101.

(42) Gunstensen, A.; Rothman, D.; Zaleski, S.; Zanetti, G. Lattice Boltzmann model of immiscible fluids. *Phys. Rev. A* **1991**, *43*, 4320–4327.

(43) Latva-Kokko, M.; Rothman, D. Diffusion properties of gradient-based lattice Boltzmann models of immiscible fluids. *Phys. Rev. E* **2005**, *71*, 056702.

(44) Liu, H.; Valocchi, A.; Kang, Q. Three-dimensional lattice Boltzmann model for immiscible two-phase flow simulations. *Phys. Rev. E* **2012**, *85*, 046309.

(45) Wu, L.; Tsutahara, M.; Kim, L.; Ha, M. Three-dimensional lattice Boltzmann simulations of droplet formation in a cross-junction microchannel. *Int. J. Multiphase Flow* **2008**, *34*, 852–864.

(46) Liu, H.; Zhang, Y. Droplet formation in microfluidic cross-junctions. *Phys. Fluids* **2011**, *23*, 082101.

(47) Benzi, R.; Succi, S.; Vergassola, M. The lattice Boltzmann equation: Theory and applications. *Phys. Rep.* **1992**, *222*, 145–197.

(48) Chen, S.; Doolen, G. Lattice Boltzmann Method for Fluid Flows. *Annu. Rev. Fluid Mech.* **1998**, *30*, 329–364.

(49) Aidun, C.; Clausen, J. Lattice-Boltzmann Method for Complex Flows. *Annu. Rev. Fluid Mech.* **2010**, *42*, 439–472.

(50) Falcucci, G.; Ubertini, S.; Biscarini, C.; Di Francesco, S.; Chiappini, D.; Palpacelli, S.; De Maio, A.; Succi, S. Lattice Boltzmann methods for multiphase flow simulations across scales. *Commun. Comput. Phys.* **2011**, *9*, 269–296.

(51) Pooley, C.; Furtado, K. Eliminating spurious velocities in the free-energy lattice Boltzmann method. *Phys. Rev. E* **2008**, *77*, 046702.

(52) Shardt, O.; Derksen, J.; Mitra, S. Simulations of droplet collisions in shear flow. Proceedings of the ASME 2012 International Mechanical Engineering Congress & Exposition. 2012.

(53) Ladd, A. Numerical simulations of particulate suspensions via a discretized Boltzmann equation. Part 1. Theoretical foundation. *J. Fluid Mech.* **1994**, *271*, 285–309.

(54) Zou, Q.; He, X. On pressure and velocity boundary conditions for the lattice Boltzmann BGK model. *Phys. Fluids* **1997**, *9*, 1591–1598.

(55) Paulsen, J.; Burton, J.; Nagel, S. Viscous to Interial Crossover in Liquid Drop Coalescence. *Phys. Rev. Lett.* **2011**, *106*, 114501.

(56) Lee, T.; Fischer, P. Eliminating parasitic currents in the lattice Boltzmann equation method for nonideal gases. *Phys. Rev. E* **2006**, *74*, 046709.

(57) Duchemin, L.; Eggers, J.; Josserand, C. Inviscid coalescence of drops. *J. Fluid Mech.* **2003**, *487*, 167–178.

(58) Yue, P.; Feng, J. Can diffuse-interface models quantitatively describe moving contact lines? *Eur. Phys. J. Special Topics* **2011**, *197*, 37–46.

(59) Yao, W.; Maris, H.; Pennington, P.; Seidel, G. Coalescence of viscous liquid drops. *Phys. Rev. E* **2005**, *71*, 016309.

(60) Ceniceros, H.; Nós, R.; Roma, A. Three-dimensional, fully adaptive simulations of phase-field fluid models. *J. Comp. Phys.* **2010**, *229*, 6135–6155.

Graphical TOC Entry